THE GEOPHYSICAL INSTITUTE OF ISRAEL המכון הגיאופיסי לישראל
P.O.B. 182, LOD 71100, ISRAEL, TEL: 972-8-9785888, FAX: 972-8-9208811 - רח' הבעש"ט 6, לוד
www.gii.co.il

SITE EFFECT AND MICROZONATION OF THE COASTAL PLAIN FROM NORTHERN AKKO TO NAHARIYYA FOR THE ASSESSMENT OF EARTHQUAKE HAZARD

Final Report

November, 2010 **Report No 533/545/10**

Principal Investigator:

Dr. A. Hofstetter

Collaborators:

T. Aksinenko, V. Giller, A. Shvartsburg, D. Giller, I. Dan, G. Ataev, M. Gorstein, N. Perelman and M. Kalmanovich

Prepared for
The Steering Committee for
National Earthquake Preparedness

TABLE OF CONTENTS

LIST OF FIGURES 2

LIST OF TABLES 3

ABSTRACT 4

1. INTRODUCTION 5

2. GEOLOGICAL BACKGROUND 7

2.1. Stratigraphy and lithology 7

3. OBSERVATIONS 11

4. DATA PROCESSING. 13

5. THE MECHANICAL PROPERTIES OF THE SUBSURFACE LAYERS IN THE INVESTIGATED AREA. 14

6. RECONSTRUCTION OF SUBSURFACE STRUCTURE ALONG PROFILES 15

7. DISTRIBUTION OF H/V RESONANCE FREQUENCIES AND THEIR ASSOCIATED AMPLITUDE LEVELS 20

8. ESTIMATING THE DEPTH OF THE MAIN REFLECTOR 25

9. APPING THE THICKNESS OF SEDIMENTS HEFER FORMATION (SIVAN, 1996) AND THEIR AVERAGE SHEAR-WAVE VELOCITY 27

10. SEISMIC HAZARD MICROZONATION 30

CONCLUSIONS 35

ACKNOWLEDGMENTS 36

REFERENCES 37

LIST OF FIGURES

Figure 1. Geological map from Sneh (2004) with measuring sites location 8
Figure 2. Schematic cross section of the Quaternary sequence on the Calilee coastal plain (Sivan, 1996 and Sivan, Gvirtzman and Sass, 1997) 10
Figure 3 Examples of locations of seismic stations in the study area 12
Figure 4 Geological map with wells and cross-sections location 17
Figure 5 Schematic geological NS cross sections beneath profiles A, B, C and D 18
Figure 6 Comparison between the analytical transfer function (black dashed line) and experimental H/V spectral ratio (red line) obtained at sites along profiles A, B, C and D. 19
Figure 7 Amplitude at the fundamental frequency vs. modeled sediment thickness above reflector. 21
Figure 8 Distribution of the fundamental frequency (a) and its associated amplitude (b) 22
Figure 9 Comparison of the faults detected by the H/V analysis with those mapped by Mero (1983) Sivan (1996) and Fleisher and Gafsou (2003) 23
Figure 10 the H/V resonance frequency correlated with thickness of sediments above Kurdani Fm. or prior formations (a) and its associated amplitude (b) 24
Figure 11 Fundamental frequency vs. modeled sediment thickness above reflector 25
Figure 12 Reflector depth inferred from microtremor measurement analysis 26
Figure 13 The thickness of sediments Hefer formations (a) and their average shear-wave velocity (b) obtained from microtremor measurement analysis 28
Figure 14 Comparison between the analytical transfer function (black dashed line) and experimental H/V spectral ratio (red line) obtained at sites are shown in Figure 13 29
Figure 15 Seismic microzoning map of Nahariyya area 31
Figure 16 Spectral accelerations for each zone. Spectrum according to the Israel Building Code (PGA of 0.093) is indicated by the dashed line (included for reference) 34

LIST OF TABLES

Table 1 Seismic station characteristics 12
Table 2 Mechanical properties of the materials used in the 1D model 15
Table 3 Soil column models for representative sites of zones 32

ABSTRACT

Over the years, we have conducted site investigations in several thousands of sites across Israel. These investigations demonstrate the usefulness of using horizontal-to-vertical (H/V) spectral ratios from ambient noise measurements to identify sites with high potential for being vulnerable to amplification effects and characterize the sites with respect to their expected resonance frequencies and the corresponding H/V levels. This information, together with any available geological, geotechnical and geophysical information, helps building a reliable model of the subsurface, which is then integrated in the processes of the seismic hazard assessment.

In the present study 164 ambient noise measurements in grid 0.5 km were carried out in the area of 34.1 km2 including the town Nahariyya. Our investigation demonstrates that the H/V curves exhibit two and more resonance peaks appearing at different frequencies. The corresponding frequencies are interpreted as fundamental (f_0) and other natural (f_n). The first fundamental peak (f_0) is associated with a deeper reflector. The second peak (f_1) correlated with thickness of sediments above shallow reflector. The amplitude of other resonance peaks depends mainly on intermediate impedance contrasts. We present four maps that reflect the fundamental characteristics of site effects in the area: dominant frequencies and maximum relative amplifications.

Using the data of the observed resonance frequencies, their associated amplitude across the investigated area, we constructed a subsurface multilayer models, estimated the thickness of the sediments at all of the measurement sites and constructed a maps of the fundamental reflector depth, thickness and average shear-wave velocity of the sediments above shallow reflector.

The evaluated subsurface models are introduced using SEEH procedure of Shapira and van Eck (1993) to assess Uniform Hazard Site-Specific Acceleration Spectra at the investigated sites. We divided the study area into zones and characterized each of them with a generalized soil column model. Thus the seismic hazard zonation map obtained are closely tied to site effects actually measured, and therefore may lead to realistic site-specific seismic hazard assessment in Nahariyya area, in spite of the borehole, refraction data and other subsurface information paucity.

1. INTRODUCTION

The State of Israel is situated along the Dead Sea Transform (DST), which is a tectonically active plate boundary (Garfunkel, 1981; Ben-Menahem, 1991) separating the Arabian plate and the Sinai sub-plate. The DST has been generating intensive earthquake activity affecting the Israeli region. Historical catalogs (Guidoboni et al., 1994; Guidoboni and Comastri, 2005; Ambraseys, 2009) demonstrate that devastating earthquakes hit Israeli premises in the past two thousand years. According to the historical records, almost every major city in Israel was damaged several times in the last two millennia by earthquakes, including Jerusalem (e.g., Salamon et al. 2009; Avni, 1999) and is still vulnerable to the effects of an earthquake (Katz, 2004; Tavron et al., 2007; Salamon et al., 2009). The earthquake of October 30, 1759, (Amiran at al., 1994), located probably in southern Lebanon, affected most of today Lebanon, Israel and Syria with damages extended as south as Jaffa. Some sources report a death toll of 10,000-40,000 people. The earthquake that occurred on January 1, 1837, was the strongest earthquake to occur in the region since the 19-th century (Amiran et al., 1994). odern writers locate the event just north of Safed in Israel and assign to it a magnitude of 6.4 (Vered and Striem, 1976, 1977; Ben-Menahem, 1979; Amiran et al, 1994). Destruction or heavy damage was done along a relatively narrow zone which extended from the coastal area to Lake Tiberias. The Jericho earthquake of 11 July 1927 with magnitude M=6.2, was the most destructive regional seismic event in the 20-th century. The effects of the earthquake were devastating, particularly in Jerusalem and in the towns of Lod and Ramle. In Lod and Ramle, which at that time were small towns, many buildings were destroyed and 50 people were killed (Avni et al., 2002). We note that these towns are relatively distant from the epicentre, i.e., about 60 km. According to Amiran (1994), the ancient city of Acre (Akko) has been heavily damaged by earthquakes and tsunami in 881/882, 1202, 1303, 1759 and 1949.

Several well known examples of destructive earthquakes during the last three decades like the Mexico City, 1985 (Reinoso and Ordaz, 1999), Spitak, Armenia, 1988 (Borcherdt et al., 1989), California, Loma Prieta, 1989 (Hough et al., 1990) and Northridge, 1994 (Hartzell et al., 1996), Kobe, Japan, 1995 (Iwata, et al., 1996), Kocaeli (Izmit), Turkey, 1999 (Ozel et al., 2002) and Algeria, 2003 (Hamdache et al., 2004) have clearly shown that local site conditions are an important factor in determining the seismic hazard specific to a given site. This is particularly important for the areas where the sedimentary basin with strong

impedance contrast between the soft sediments and the underlying bedrock and the soil conditions vary significantly from one place to another.

Nakamura (1989) proposed the hypothesis that site response function under low strain can be determined as the spectral ratio of the horizontal versus the vertical component (H/V) of motion observed at the same site. He hypothesized that the vertical component of ambient noise is relatively unaffected by the unconsolidated near-surface layers. Some studies have used the ambient noise array method to evaluate shallow velocity structures (Liu et al., 2000, Mareska et al, 2006, Di Giulio et al., 2006, Kuo et al, 2008 and many other). In recent years different studies (Ibs-von Seht and Wohlenberg, 1999; Delgado et al., 2000; Kobayashi et al., 2000; Parolai et al., 2002; Hinzen et al., 2004; García-Jerez et al., 2006) showed that the resonance frequency of the site obtained from horizontal-to-vertical spectral ratios of ambient vibration can be used to map the thickness of soft sediments.

During 2005-2009, ambient noise measurements (Zaslavsky et. al., 2006a, 2006b 2007a, 2007b, 2008 and 2009; Hofstetter et. al., 2008) were conducted at 1488 locations in an area of about 220.7 km2 including Emek Zevulun and a southern part Western Galilee coastal plain. The result has shown two H/V peaks at frequencies related to resonances of deep and shallow structures. Spatial variations of the frequency 0.4-5 Hz for the first peak and 1-8 Hz for the second peak, and H/V amplitude level of 2-5 for the first peak and 2-10 for the second peak, reflected a complex geological structure of the studied area.

In this report we continue investigation of seismic hazard to the northern part of the Western Galilee coastal plain including the town of Nahariyya and adjoining settlements. This study focused on the following objectives:

1. Empirical evaluation of potential enhanced ground motion in soft sediments using dense grid recording of ambient noise. Reliable prediction of site amplification in the investigated area and producing maps of the distribution of the fundamental frequency and amplification.
2. Integrated analysis of microtremor measurement results and available geological, borehole to reconstruct the subsurface structure.
3. Identifying, and estimating vertical displacement of faults, which are defined as a discontinuity in the subsurface model and associated with: (1) a sharp shift in the fundamental frequency corresponding to a vertical displacement; (2) significant difference in all three characteristics of the H/V spectra, i.e. fundamental frequency, amplitude and shape corresponding to both vertical displacement and change in the velocity profile.

4. Use of the adequate analytical transfer functions and Stochastic Evaluation of Earthquake Hazard for prediction the site dependent Seismic Ground-Motion Hazard Maps in terms of ground motion parameters used for engineering purposes

2. GEOLOGICAL BACKGROUND

The study area includes the town of Nahariyya and adjoining settlements situated at the Western Galilee coastal plain. Figure 1 presents the geological map of the study area at a scale of 1:50,000 compiled from Sneh (2004) with location of the measuring sites and faults by Fleischer and Gafsou (2003). The Coastal Plain of Western Galilee (Fig. 1) is 4-7 km wide and rises gradually from sea level to about 50 m above MSL between the Mediterranean Sea in the west and the Galilee foothills in the east. A discontinuous longitudinal ridge composed of calcareous sandstone (Kurkar), rising 30-40 m above MSL exists about 2 km east of and parallel to the shoreline.

The Neogene and Pleistocene formations in this region have been previously discussed in detail by Bar Yosef (1967), by Issar and Picard (1969), Issar and Kafri (1972) and by Sivan (1996). The additional surface and subsurface data used in the present study are complied from Mero (1983) and Fleischer and Gafsou (2003).

The study area is crossed by system of faults which were interpreted from deep seismic surveys (Fleischer and Gafsou, 2003 and Mero, 1983) and were discussed by Sivan (1996).

2.1 Stratigraphy and lithology

Lithostratigraphic units recognized in this region are the Judea, Mt. Scopus, Avedat, Saqiye and Kurkar Groups (Mero, 1983; Issar and Kafri, 1972). In the Western Galilee the Judea Group is known from outcrops, boreholes and geophysical investigations. The age of the Group is Cenomanian - Turonian. The Judea Group consists of dolomites, limestone, chalks, marls and chert. The Mt. Scopus Group is composed of Senonian to Paleocene formations, cropping out in a restricted strip along the Galilee foothills and, according to Mero (1983), in the subsurface exists in most of the area. The Group is composed of the Menuha, Ghareb and Taqiye Formations and represented by limy chalk,chalk, marly chalk sometimes bituminous.

The Avedat Group of Lower and Middle Eocene age is composed of the Adulam and Maresha Formations, which cover all earlier formations and in the subsurface exist in the

whole of the study area. The members are represented by alternations of chalk, chalky limestone.

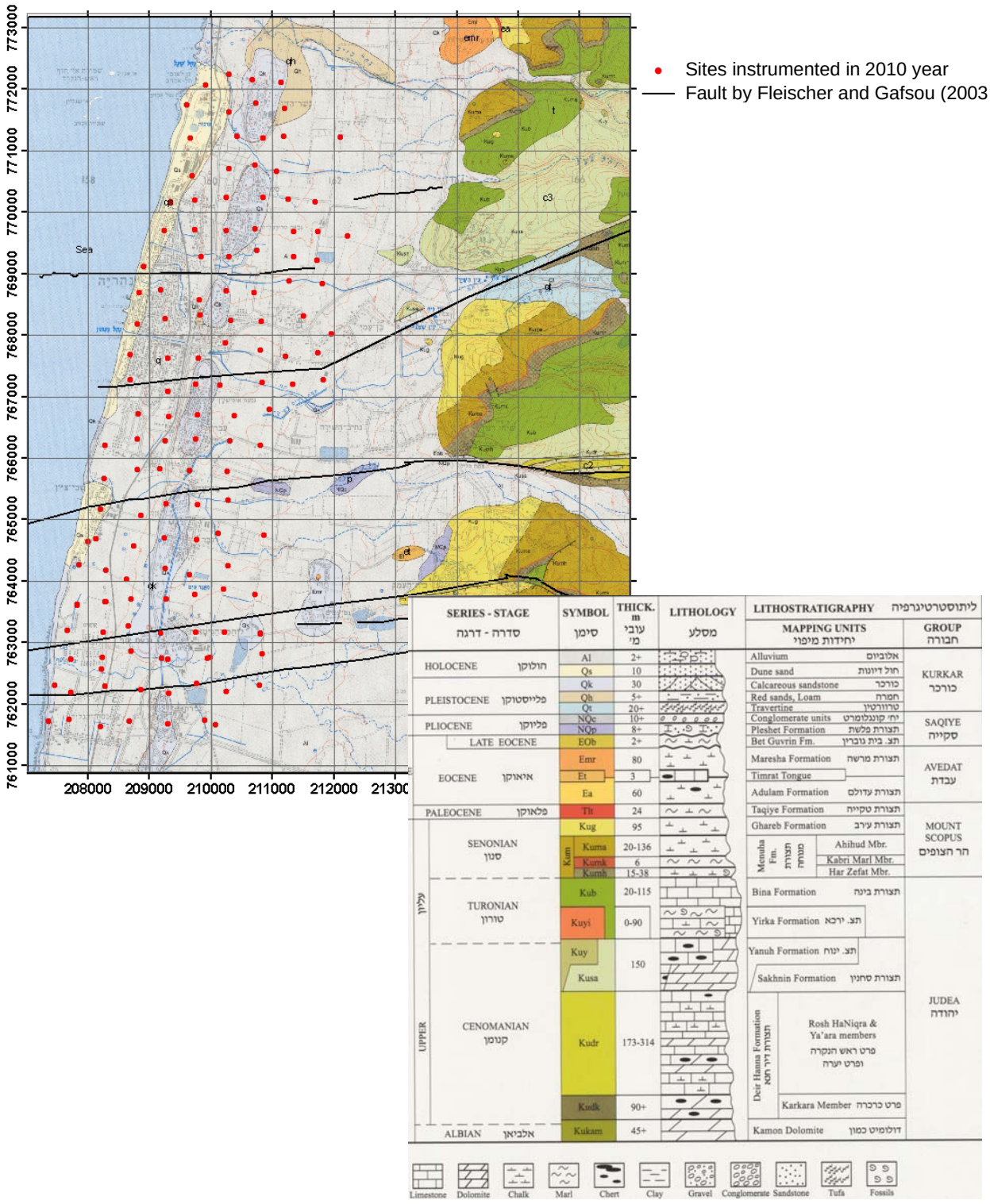

Figure 1 Geological map from Sneh (2004) with measuring sites location.

The Saqiye Group overlies the Mt, Scopus and Avedat Groups uncomfortably and is overlain by the Kurkar Group. The Saqiye Group in the study area is composed of the Bet Guvrin (Upper Eocene - Early Miocene) and Yafo (Upper Miocene to Pliocene) Formations. Bet Guvrin Formation overlies the Maresha Formations of the Avedat Groups conformably. It is unconformably overlain by the Yafo Formation (Upper Miocene to Pliocene). Near the Naharia Horst it is overlain by younger formations of the Kurkar Group. In the subsurface it occurs in the study area, but disappears towards the east. The Bet Guvrin Formation is represented by chalk and marl. In a few places it occurs as fine bioclastic limestone lenses with limonitic stains and chert.

Yafo Formation of Upper Miocene to Pliocene age overlies the Bet Guvrin Formation unconformably and is overlain by the Kurkar Group. Formation is represented by marls.

Sivan (1996) and Sivan et al. (1997) divide the Quaternary sequence (Kurkar Group) into the Kurdane and Hefer formations (Fig. 2).

The Kurdane Formation consists mainly of calcareous sandstone and sandy limestone. The Formation unconformably overlies the Saqiye Group in the western part of the study area, and Avedat and Mt. Scopus Groups along the eastern side.

The Hefer Formation, which consists of the Pleistocene and Holocene sequences unconformably overlies the Kurdane Formation and is subdivided into members:

- Nes Amim Member consists of a discontinuous paleosol (hamra) layer between the Kurdane and Akko kurkar. The hamra consists of sand, with varying amounts of clay. Pebbles are an additional component in the northeast of the area.
- Akko Member consists of sandy calcarenites, coarsegrained and poorly sorted in the west and finer and well-sorted in the east.
- Evron Member the thickest soil unit in the Quaternary sequence of the Galilee coastal plain. The unit is a dark red, argillaceous paleosol, with ferruginous nodules at the top that grades downward into orange, fine-grained, sandy soil.
- Regba Member consists of two kurkar units and an interbedded hamra horizon. It occurs characteristically in three longitudinal north–south kurkar ridges, two of which (the Evron and the coastal ridges) are found on land, while the third is mostly submerged. This unit also occurs in flat areas east of the Evron ridge.
- Ga'aton Member consists predominantly of dark clay. It is restricted to a few depressions along the coast, in particular east and north of Akko.

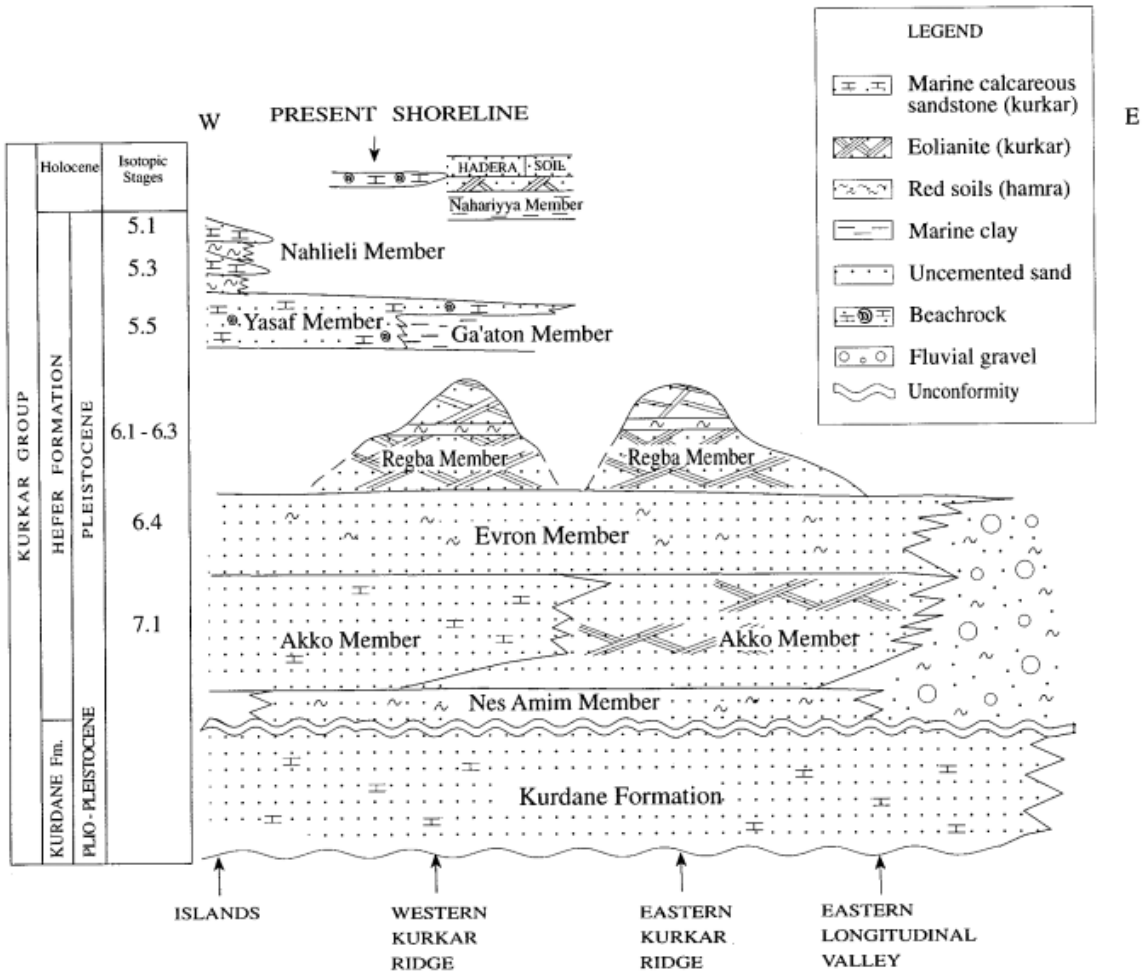

Figure 2. Schematic cross section of the Quaternary sequence on the Calilee coastal plain (Sivan, 1996; and Sivan et al., 1997).

- Yasaf Member characteristically consists of biocalcarenites. In the subsurface, the member is covered by recent clay and sand. This member is found in outcrops and in the subsurface. The Yasaf Member unconformably overlies the Regba kurkars at the coastal ridge and at the western ridge, now mostly submerged.
- The Holocene sediments include the clay of the Nahariyya Member, young eolianites, modern sand (the Hadera sand), and recent to subrecent beachrock.

Owing to their geotechnical characteristics the following lithostratigraphic units are potential reflectors in the study area:

- Top Judea Group is identified as the deep reflector;
- Top Kurdani Formation, or/and prior formations we consider as a shallow reflector.

3. OBSERVATIONS

The seismic noise recorded in urban areas of Israel can be considered as caused by human activity (cars, factories, etc.) and propagates as high-frequency waves (> 1 Hz) or by oceanic waves, which propagates over large distances in the low-frequency range (< 1 Hz). All the analyzed data were recorded using the multi-channel digital seismic data acquisition system designed for site response field investigations (see Shapira and Avirav, 1995). The data acquisition system includes: a multi-channel amplifier with band pass filters 0.2-25 Hz, GPS (for timing) and a laptop computer with a 16 bit/word analogy-to-digital (A/D) conversion card with a sampling rate of 100 samples/s. The seismometers are velocity transducers (L4C by Mark Products) with a natural frequency of 1.0 Hz and damping at 70% of critical. All the equipment: sensors, power supply, amplifiers, personal computer and connectors are carried in a vehicle, which also serves as a recording centre. The seismometers are fixed on levelled metal plate placed directly on the ground. Prior to performing measurements, the individual seismometer constants (natural frequency, damping and motor constant) are determined using sine and step calibration signals, and then the frequency response functions of all channels are computed. This procedure allows evaluating change of natural frequency and motor constant (voltage sensitivity) during long time of measurements in harsh conditions in the free field. The seismic stations characteristics are presented in Table 1. In the final instrumental test, all seismometers are placed at the same location and in the same orientation to record the same waves.

Normally the differences between the seismic channels are marginal even without "correcting" for the instrumentation response. In fact, at frequencies below the natural frequency of the seismometers, correcting for the instrument response may increase variability and scattering. We note that all channels (horizontal and vertical) have practically the same frequency response function and amplifiers are set to the same gain level. Hence, spectral ratio may be calculated on the recorded signals. Moreover, it is possible to assess the predominant frequencies in the H/V spectra also at frequencies much lower than the natural frequency of the seismometer.

We carried out 164 ambient noise measurements from December 22, 2009, to April 27, 2010. The work area is approximately 34.1 km^2. The locations of measurement points are shown in Figure 1. In Figure 3 we present examples of the locations of the seismic stations at different soil units and in the urban area during the site investigations in the Nahariyya area.

Figure 3. Examples of locations of seismic stations in the study area.

Table 1 Seismic station characteristics.

Site Number	Sensor Number	Component	Code	Generator Const. at 1 Hz V/m/sec	Frequency Hz	Damping %
1-82	3225	Vertical	V405	94.8	1.00	70

	3210	Horizontal (NS)	H558	123.3	1.00	68
	3401	Horizontal (EW)	H749	123.1	1.00	64
83 - 104	3225	Vertical	V225	121.55	1.00	70
	3396	Horizontal (NS)	H396	105.34	1.00	70
	3401	Horizontal (EW)	H401	116.07	1.00	65
105 - 164	3225	Vertical	V407	103	1.00	67
	3396	Horizontal (NS)	H558	122.51	1.00	67
	3401	Horizontal (EW)	H749	127.63	1.00	60

4. DATA PROCESSING

To study the characteristics of spectra of the ambient noise signals, we compute Fourier spectra and spectral ratios. The record length (time window) used for spectral calculations depends on the fundamental frequency. The basic criterion is to choose the minimal time window which yields spectra that practically do change when the record length is increased. We have concluded that at sites with fundamental frequencies of 1 Hz (or more) we should use a record of at least 30 sec. The selected time windows are Fourier transformed, using cosine-tapering (1 sec at each end) before transformation and then smoothed with a triangular moving Hanning window. More precisely, we apply "window closing" procedure (see Jenkins and Watts, 1969) for smart smoothing of spectral estimates so that any significant spectral peaks are not distorted.

The H/V spectral ratios are obtained by dividing the individual spectrum of each of the horizontal components [$S_{NS}(f)$ and $S_{EW}(f)$] by the spectrum of the vertical component [$S_V(f)$]:

$$A_{NS}(f) = \frac{S_{NS}(f)}{S_V(f)} \qquad A_{EW}(f) = \frac{S_{EW}(f)}{S_V(f)} \qquad (1)$$

The average spectral ratio for each of two horizontal components is computed, if the curves of average spectral ratios of the two components are similar then the average of the two horizontal-to-vertical ratios is defined as:

$$A(f)=\frac{1}{2n}\left[\sum_{i=1}^{n}\frac{S_{NS}(f)_i}{S_V(f)_i}+\sum_{i=1}^{n}\frac{S_{EW}(f)_i}{S_V(f)_i}\right] \qquad (2)$$

The length of recorded ground motions (ambient noise) may affect the results and influence the reliability and applicability of the technique. According to Teves Costa et al. (1996), Teves Costa and Senos (2000), Dravinski et al. (2003) a total ambient noise recording of five minutes is sufficient. Lebrun et al. (2004) and Garcia- Jerez et al. (2006) advocated recording time of 10 minutes, while many authors (e.g., Parolai et al., 2002; Ferretti et al., 2007, and others) suggest that signals should be recorded for at least 30 minutes. From comparison between the average H/V curves obtained from ambient noise recordings of different durations we conclude that recording for about 1-2 hours provides reliable estimate of the H/V function.

5. THE MECHANICAL PROPERTIES OF THE SUBSURFACE LAYERS IN THE INVESTIGATED AREA

The necessary parameters to development analytical model for site response estimation by using SHAKE program (Schnabel et al., 1972) are the S-wave velocity of the unconsolidated sediments, thickness of each layers, density and specific attenuation in different lithological units as well as S-wave velocity and density of the reflector. Densities and specific attenuation in different lithological units are chosen on the base of literature sources (Borcherdt et al., 1989; McGarr et al., 1991; Theodulidis et al., 1996; Reinozo and Ordas, 1999; Pergalani et al., 2000 and many others).

In previous study in Zevulun plain (Zaslavsky et al., 2006 and 2009) collected data of S-velocities available from a few refraction profiles (Ezersky, 2004 and 2006) and boreholes.The S-wave velocity values of kurkar and hamra beds that recur several times in the sequence of the Hefer Formation (Kurkar Group), were obtained on the basis of integrated analysis of the microtremor measurement and the stratigraphic correlation of the Quaternary sequence (Sivan, 1996). We considered that shear wave velocities of the hamra beds is 220-450 m/sec and kurkar beds is 550-750 m/sec.

The available shallow water wells (Figure 4) (Issar and Kafri, 1972 and Sivan, 1996) penetrated only a part of the Saqiye Group. The penetrated sequence consists of chalk and marl and identified as Beit Guvrin and Yafo Formations (Gvirtzma 1970).

The H/V spectral ratios show two and more resonance peaks. The first, fundamental one is associated with the Top Judea Gr. Amplitude of the fundamental frequency is formed by the impedance contrast between the rock sequence consisting the Senonian to Neogene units and the limestone and dolomite of the Judea Gr. In most parts of the study area the amplitude varies in a range of 1.6-2.6. At the points, where the thickness of soft beds of the Kurkar Gr. is a significant part of the total sediments thickness, the average S-wave velocity of the entire sequence unconsolidated layers increases. This leads to an increase in the amplitude of the fundamental frequency of up to 2.8-4.0. We consider that the rock sequence of Senonian - Neogene lithologically almost homogeneous with Vs=950-1100 m/sec. Table 2 summarizes the mechanical properties for the subsoil layers in investigated area.

Table 2 Mechanical properties of the materials used in the 1D model

Lithological unit	**V_s** m/sec	**Density** g/cm^3	**Damping** %
Uncemented sand (Holocene)	160-200	1.5	3
Red soils (Evron and Nes Amim Members of Hefer Fm., Kurkar Gr.) Pleistocene	220-450	1.6-1.8	3
Gravels (Hefer Fm., Kurkar Gr.) Pleistocene	450-550	1.8	3
Marine calcareous sandstone (kurkar) and Eolianite (kurkar) (Yasaf, Regba, Akko Members of Hefer Fm. Kurkar Gr) Pleistocene	550-750	1.8-1.9	3
Sandy Limestone (Kurdani Fm. of Kurkar Gr) Plio-Pleistocene	1200	2	2
Chalk marl (Saqiye, Avedat and Mount Scopus Groups) Senonian- Pliocene	950-1050	2	2
Limestone and dolomite (Judea Gr., Cenomanian-Turonian)	1900	2.2	

6. RECONSTRUCTION OF SUBSURFACE STRUCTURE ALONG PROFILES

Using the data of the observed resonance frequencies, their associated amplitudes across the investigated area and the shear wave velocity values presented in Table 2, we can

construct a subsurface multilayer model and estimate the thickness of the sediments at most of the measurement sites where borehole information is not available. The constructed subsurface models are based on available geological and geophysical data and these are constrained by the empirical H/V information.

Positions of cross-sections over Nahariyya area are indicated in Figures 4. Cross-sections are shown in Figure 5 have N-S direction and illustrate the results of H/V analysis. Figure 6 depicts H/V spectral ratios for representative sites located along profiles together with the corresponding analytical transfer functions that were computed for the suggested 1D model to each site.

The H/V spectral ratios show two and more resonance peaks. The corresponding frequencies are interpreted as fundamental (f_0) and other natural (f_n). The first fundamental peak (f_0) is associated with the limestone and dolomite of the Judea Gr. The second peak (f_1) correlated with thickness of sediments above Kurdani or prior formations. The amplitude of other resonance peaks depends mainly on intermediate impedance contrasts which are associated with interbedded kurkar and hamra layers.

Results of the integrated analysis of microtremor measurement and available geological information have shown that limestone and the dolomite of the Judea Gr. is a fundamental reflector. The wide range of the first resonance frequency (0.4 Hz to 1.7 Hz along profile A, 0.55 Hz to 2.0 Hz along profile B, 0.55 Hz to 4.0 Hz along profile C, 0.65 Hz to 4.0 Hz along profile D) reflects changes in the depth of the Top Judea Gr. The sharp shift in the fundamental frequency between some neighboring points corresponds to a vertical displacement. Our investigation has allowed specifying faults defined earlier and to identify some new faults.

The structural configuration revealed by wide range of fundamental frequencies is graben and horst system. In a southern part of all profiles a horst is traced (Bustan Horst by Sivan (1996)). In profiles A and C this structure splits into two segments. We consider that the insufficient number of points does not allow us identifying on the profile B the fault which is traced between the points NHR5 and NHR6 of profile A, between the points NHR17 and NHR144 of profile C and between the points NHR138 and NHR146 of the profile D. The fault which bounds Beit HaEmek Graben (Sivan (1996) on the southern side is identified by a sharp shift in the fundamental frequency between points NHR129 and NHR128 of profile A, NHR21 and NHR25 of profile B and NHR127 and NHR28 of profile C. We consider that we did not manage to trace this fault on profile D as more dense network of measurements is

required in this part of the study area. Towards the north the graben is bounded by two downstepping horst blocks.

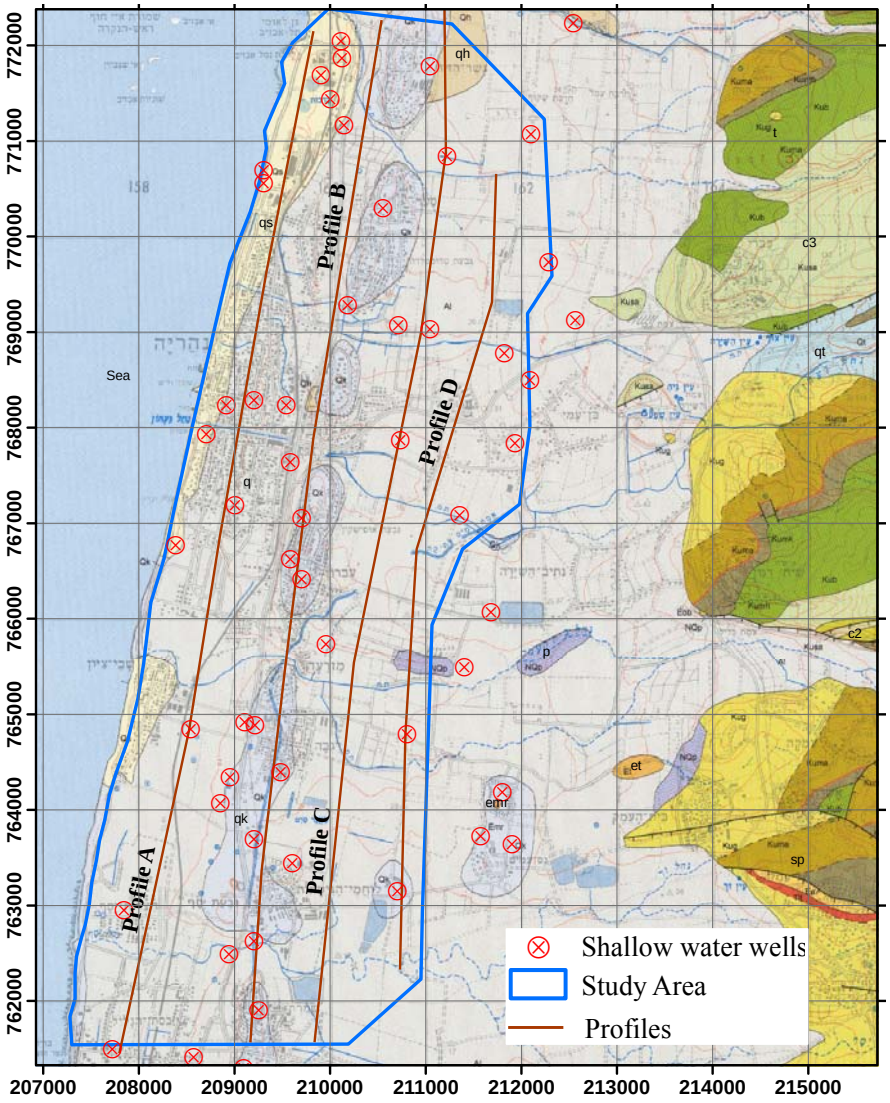

Figure 4 Geological map with wells and cross-sections location.

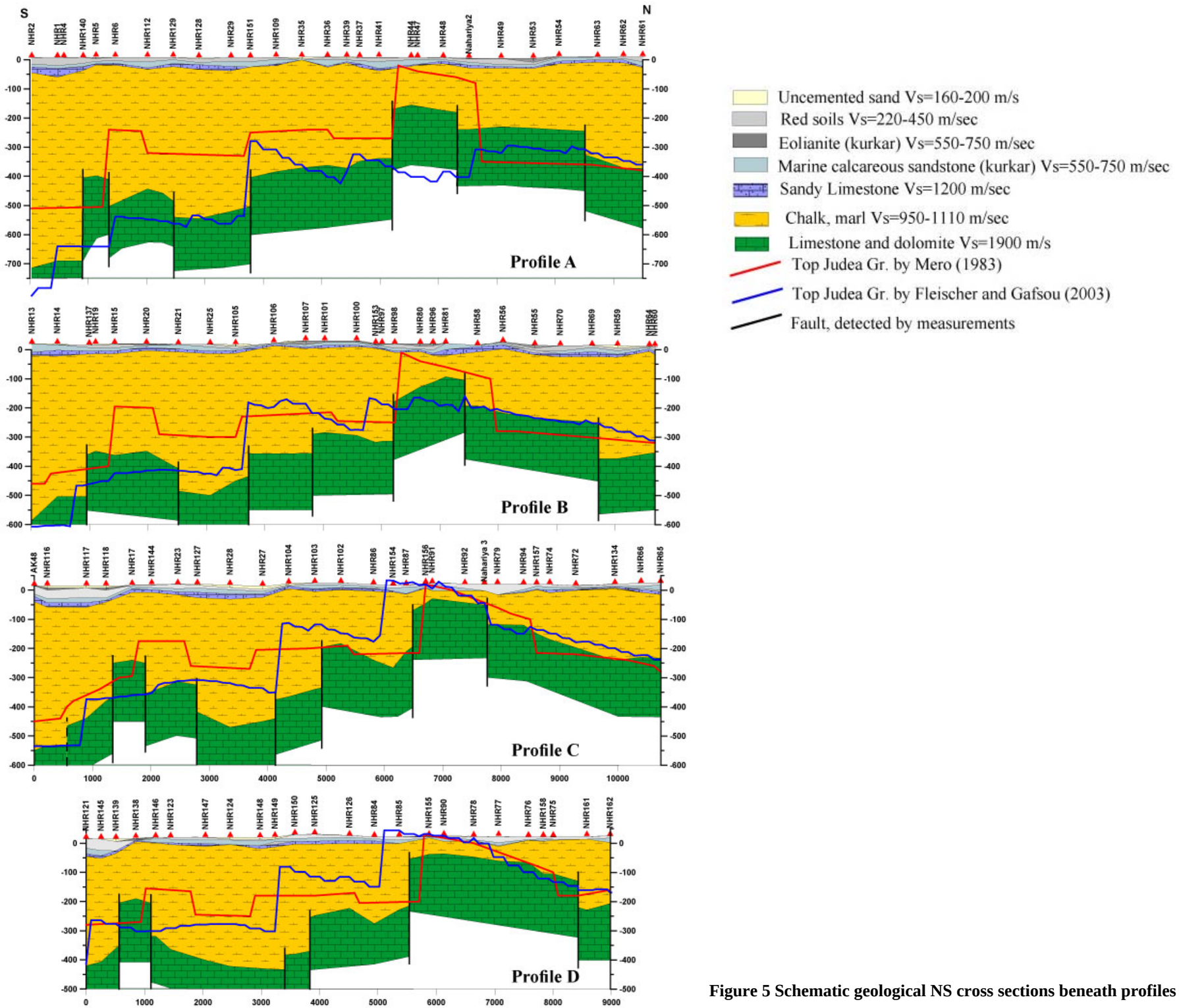

Figure 5 Schematic geological NS cross sections beneath profiles A, B, C and D.

.

Profile A

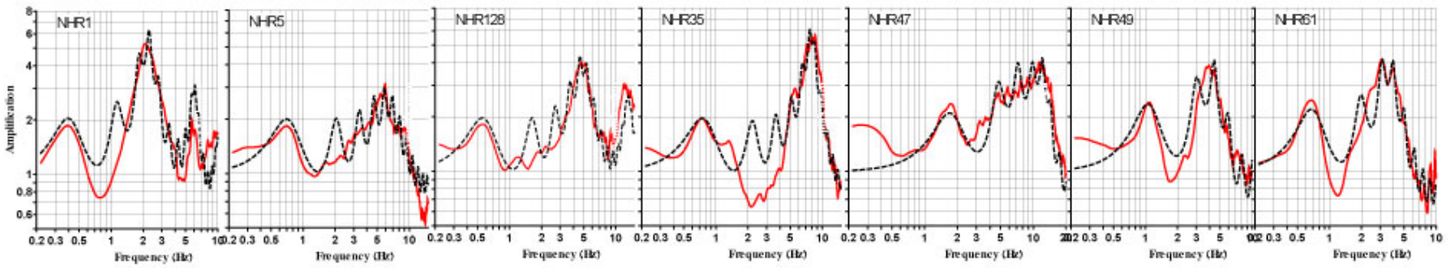

Profile B

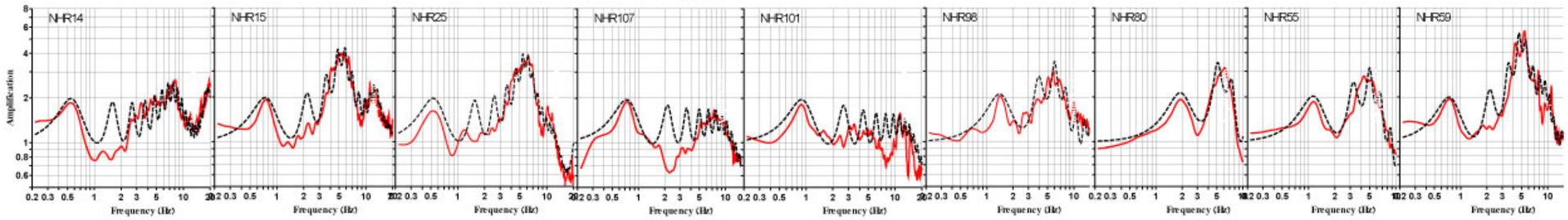

Profile C

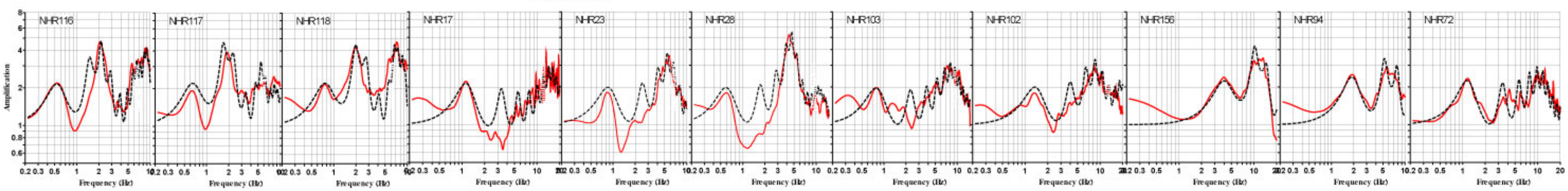

Profile D

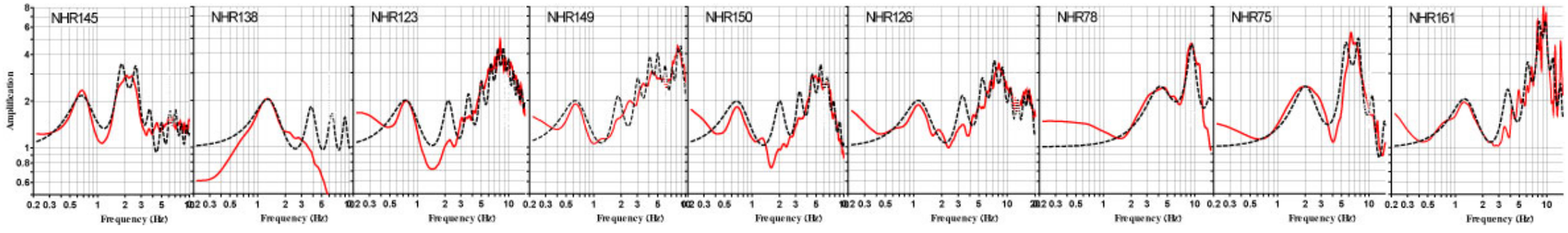

Figure 6 Comparison between the analytical transfer function (black dashed line) and experimental H/V spectral ratio (red line) obtained at sites along profiles A, B, C and D.

Sharp increase in the fundamental frequency from 0.7 Hz to 1.0 Hz between points NHR150 and NHR125 of profile D, corresponds to the decrease in the reflector depth from 420 m to 280 m respectively. Between points NHR103 and NHR102 of profile C we observe sharp increase in the fundamental frequency from 0.8 Hz to 1.3 Hz. Depth of the reflector varies from 360 m to 210 m. Between points NHR107 and NHR101 of profile B the fundamental frequency varies not considerably from 0.75 Hz to 0.9 Hz. This corresponds to a vertical displacement of 70 m. In the segment of profile A between points NHR151 and NHR41 the sharp variation of the fundamental frequency is not observed. We consider that towards the west the fault gradually disappears.

In the northwest part of the study area horst is bounded by step faults. The first fault is identified by sharp shift in the fundamental frequency between points NHR48 and Naharia 2 of profile A, NHR81 and NHR58 of profile B and Nahariya 3 and NHR79 of profile C. The second fault is identified between points NHR54 and NHR63 of profile A and points NHR69 and NHR59 of profile B. We consider that on east of the study area these faults disappear.

Sharp decrease in the fundamental frequency from 2.0 Hz to 1.25 Hz between the points NHR75 and NHR161 of profile D, corresponds to the dipping of the Top Judea from 125 m to 225 m respectively. We consider that in this part of study area appears fault.

Thicknesses and the shear wave velocity values of kurkar and hamra layers (Hefer Formation by Sivan (1996)) vary along the profiles. This is associated with high variability in the second and the other peaks appearing at different frequencies (Fig. 6).

7. DISTRIBUTION OF H/V RESONANCE FREQUENCIES AND THEIR ASSOCIATED AMPLITUDE LEVELS

Figure 8 presents maps of the contoured fundamental resonance frequency (f_0) and the associated H/V amplitude. The data exhibit peaks changing from 1.6 to 4, occurring at frequencies 0.4 -4.5 Hz. The distribution of the fundamental frequency follows the morphology of the top Judea Gr. and reflects the complicated blocks structure. Increase of the fundamental frequency north and west characterizes decrease in the depth of the Top Judea. The zone of high frequencies (1.4-4.5 Hz) detect the Horst which corresponds to uplifted block contoured in the Structural maps of the Top Judea Gr. (Fleisher and Gafsou, 2003; and Mero, 1983).

Amplitude at the fundamental H/V peak reflecting impedance contrast between deposits and fundamental reflector (Judea Gr.). As shown in Figure 7 this parameter is influenced by the thickness and average S-wave velocity of the sediments which overlay the Top Judea Gr.

In the area of the horst, thickness of soft layers of the Kurkar Gr. is a significant part of the total sediments thickness. This leads to an increase in the average S-wave velocity of the entire sequence unconsolidated sediments and hence to an increase in the amplitude of the fundamental frequency.

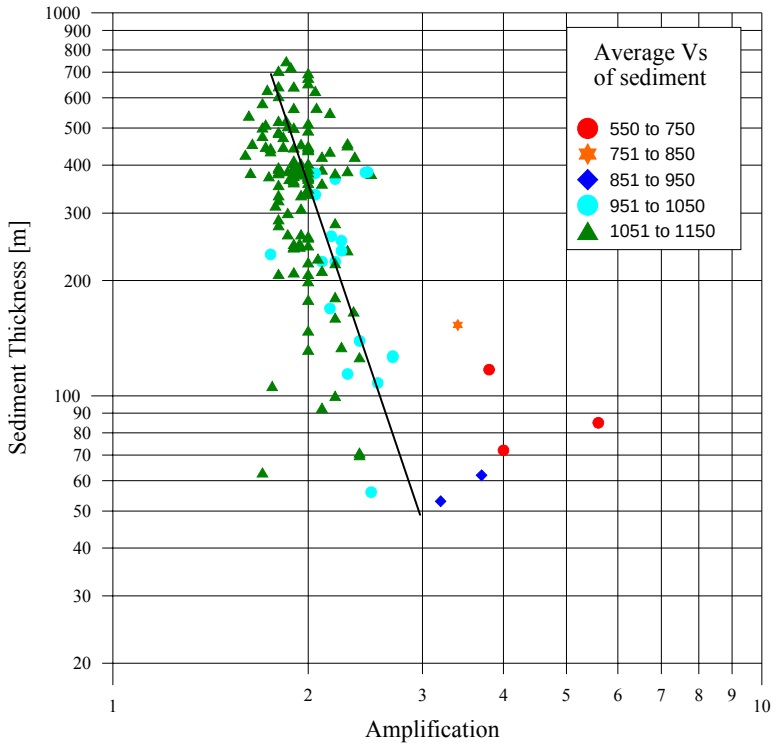

Figure 7 Amplitude at the fundamental frequency vs. modeled sediment thickness above reflector.

In our study we reconstruct the faults previously traced by geological data and reveal some new. We note the considerable differences in determining the location and direction of the faults mapped by Mero (1983), Sivan (1996), and by Fleischer and Gafsou (2003). We hope that our work will improve the accuracy of the faults mapping. A higher density of H/V measurements would allow us to more accurately trace faults and identify new faults. Figure 9 presents faults, inferred from the analysis of ambient vibration measurements and faults, mapped by Mero (1983), Sivan (1996) and by Fleischer and Gafsou (2003).

As noted above and can be seen in Figure 6, the H/V spectral ratios show two and more resonance peaks. The second peak (f_1) correlated with thickness of sediments above Kurdani or prior formations (Hefer Formation by Sivan (1996)). Figure 10 presents maps of the H/V resonance frequency correlated with thickness of the Hefer Formation sediments (f_1) and the associated H/V amplitude.

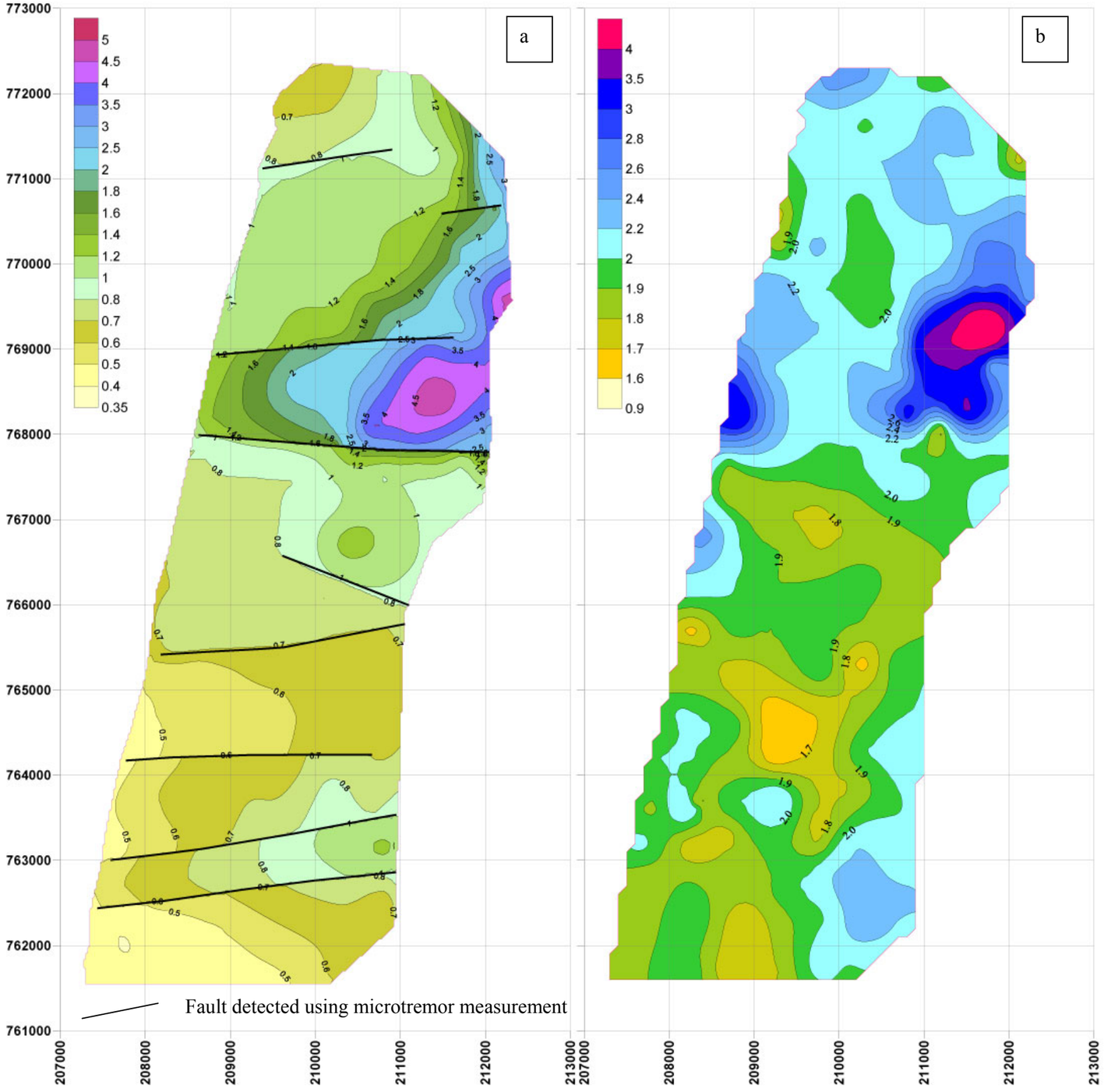

Figure 8 Distribution of the fundamental frequency (a) and its associated amplitude (b).

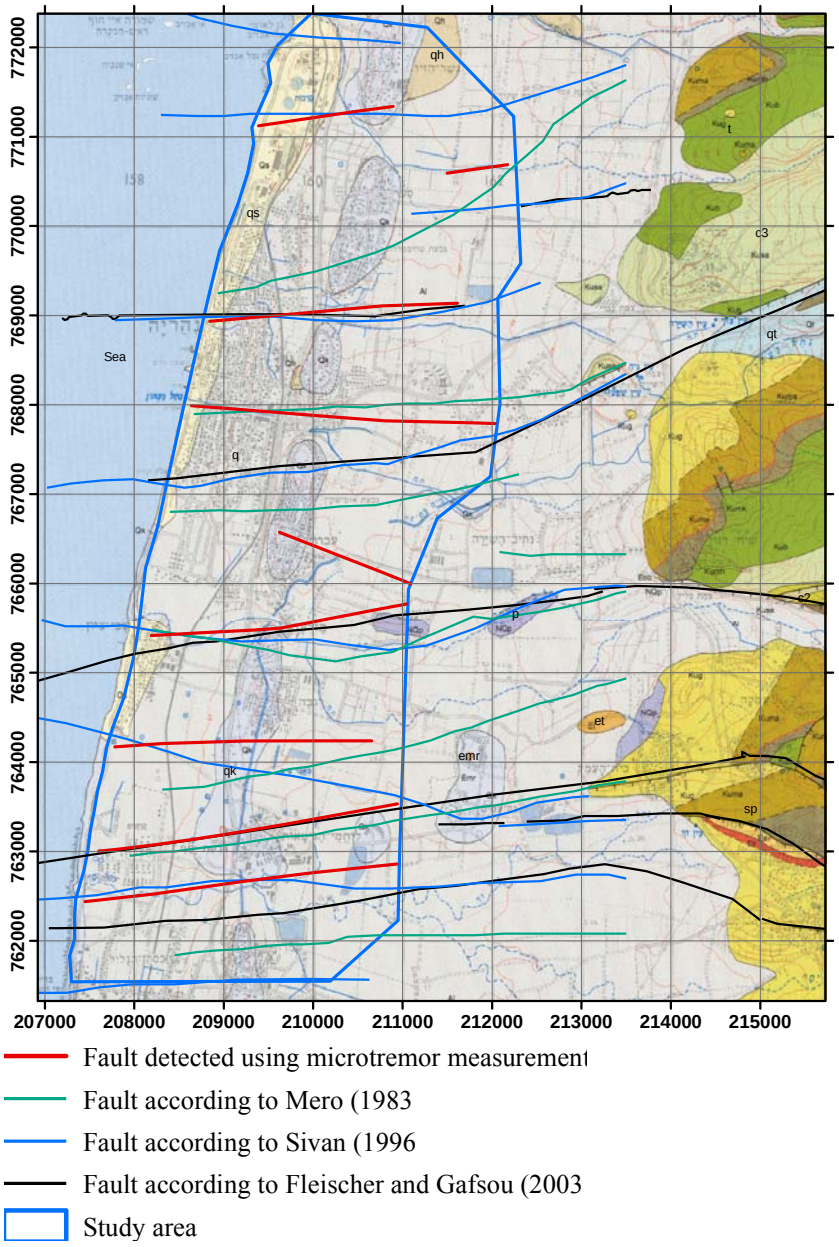

Figure 9 Comparison of the faults detected by the H/V analysis with those mapped by Mero (1983), Sivan (1996) and Fleischer and Gafsou (2003).

The data exhibit peaks changing from 2.0 to 8, occurring at frequencies 1.5 -20.0 Hz. The maps (Fig. 10) display two north-south longitudinal strips, which are characterized by high frequency (8.0-20.0 Hz) and low amplitude (2.0-2.5), or absence of the second resonance frequency. These zones are correlated with two longitudinal north-south kurkar ridges (the Evron and the coastal ridges). Between the ridges, areas with frequency of 3.0-5.0 Hz and an amplitude of 3-8 are found. The range of the second resonance frequency East of the Evron ridge is 1.5-10 Hz and its associated amplitude level is 2.5-6.0.

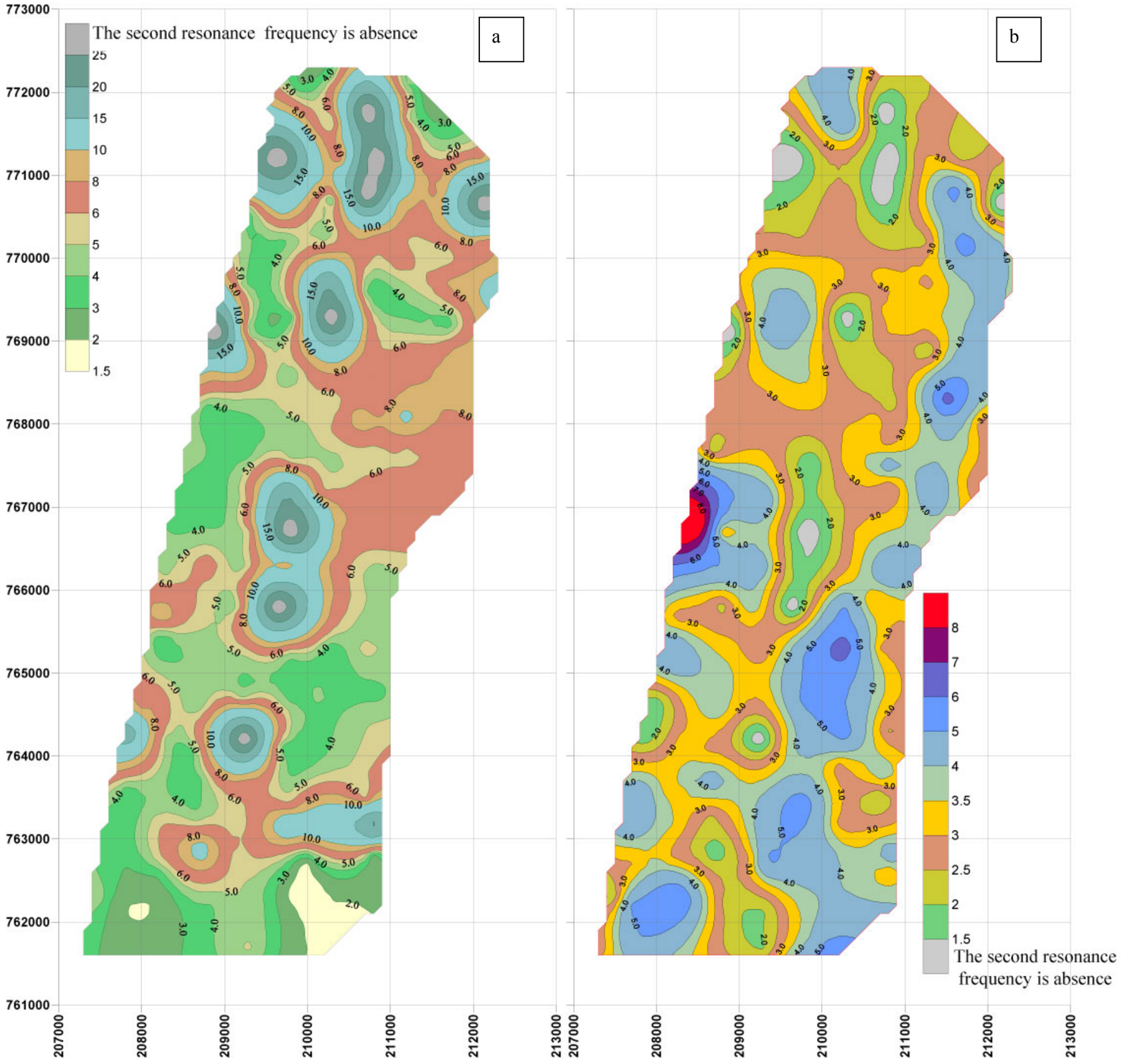

Figure 10. The H/V resonance frequency correlated with thickness of sediments above Kurdani Fm. or prior formations (a) and its associated amplitude (b).

8. ESTIMATING THE DEPTH OF THE MAIN REFLECTOR

As noted above, the first resonant frequency (f_0) is associated with limestone and dolomite of the Judea Gr., which is a fundamental reflector. Using the data of the observed resonance frequencies, their associated amplitude across the investigated area, we constructed a subsurface multilayer models, estimated the thickness of the sediments at all of the measurement sites and constructed a map of the fundamental reflector depth (Fig. 12). The map shows that the structural configuration of the reflector (Top Judea gr.) is dominated by E-W oriented tilted blocks, grabens and horsts. The structures are bounded by sets of normal faults. Two structural domains can be distinguished in the study area: a southern deeper area and a northern shallower area.

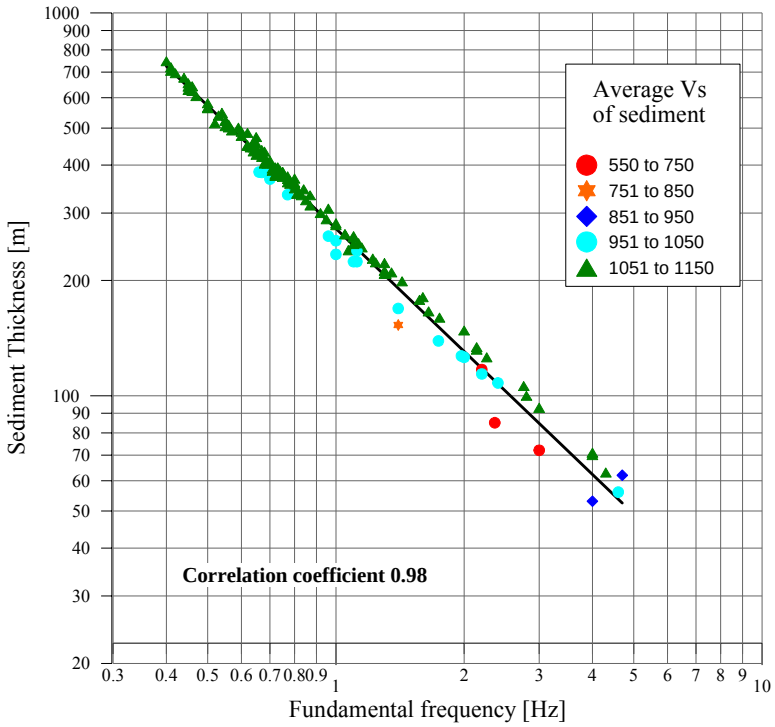

Figure 11 Fundamental frequency vs. modeled sediment thickness above reflector.

Figure 11 shows a good correlation between fundamental frequency and modeled sediment thickness with coefficient 0.98. THe thickness of soft sediments of the Kurkar Gr. in most part of study area is less than 35 meter and the rock sequence of Senonian - Neogene lithologically is almost homogeneous with Vs=950-1100 m/sec., which result in a small scatter of the parameters. Deviation from the general trend occurs if the thickness of soft

sediments (Kurkar Gr.) is a significant part of the total thickness of sediment and average S-wave velocity of sediment varies in the range of 550-850 m / sec.

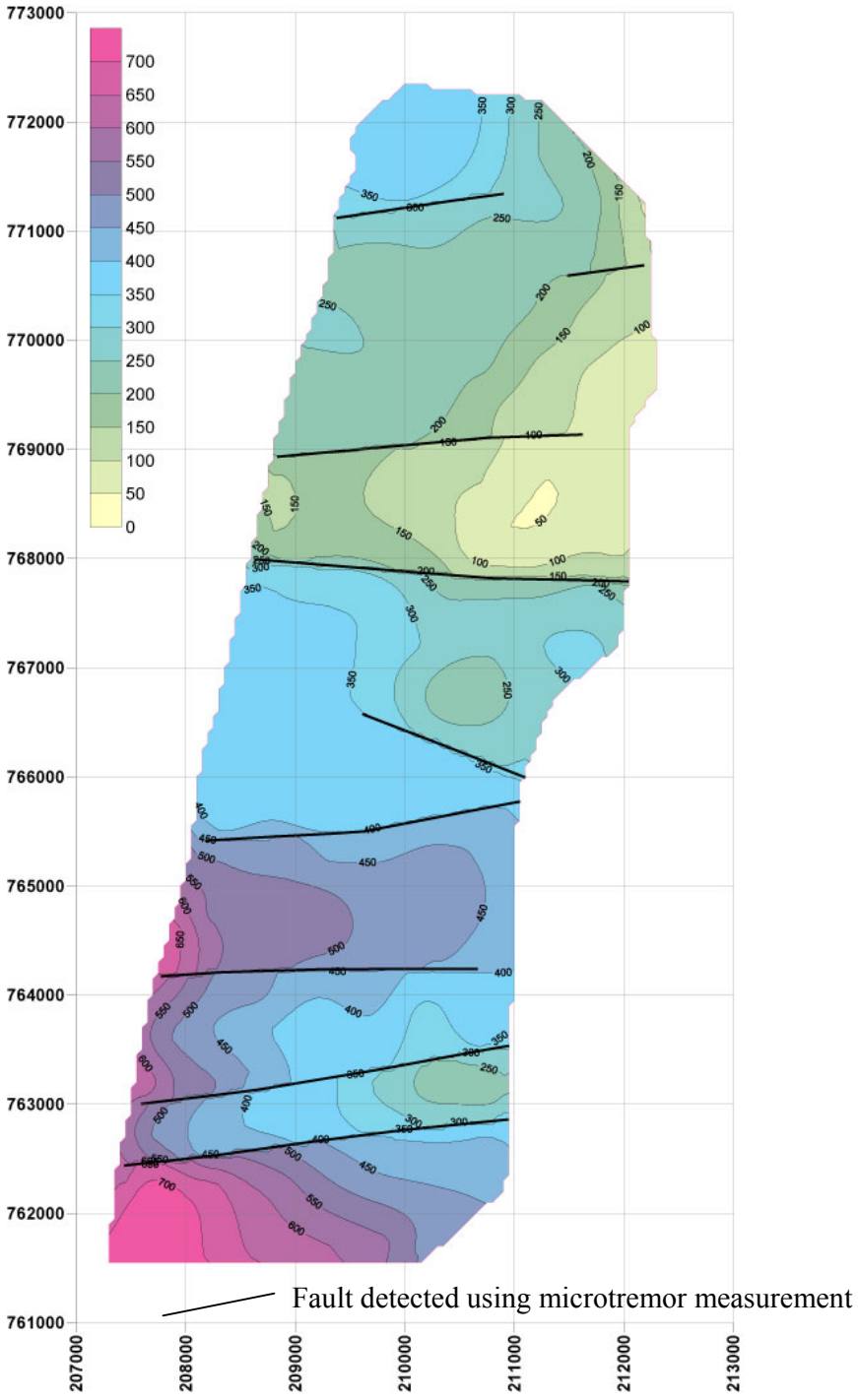

Figure 12 Reflector depth inferred from microtremor measurement analysis.

.

9. APPING THE THICKNESS OF SEDIMENTS HEFER FORMATION (SIVAN, 1996) AND THEIR AVERAGE SHEAR-WAVE VELOCITY

Accurate evaluation of ground amplification characteristics requires detailed soil profile information such as shear-wave velocity structures. Estimation of ground amplification is possible only with the shear-wave velocity of the surface layer (Borcherdt and Gibss 1976), and the amplification of strong ground motion such as peak ground velocity is correlated with the average shear-wave velocity from the surface to a certain depth (Joyner and Fumal 1984).

Geological modeling taking into account all H/V spectral ratios peaks allowed determining the thickness and the shear wave velocity values of each layer of the Hefer Formation. Using the data we constructed the maps of the thickness and average shear-wave velocity of the Hefer Formation layers (Fig. 13).

The average $\overline{Vs}$ was defined by:

$$\overline{Vs} = \frac{\sum_{i=1}^{n} di}{\sum_{i=1}^{n} \frac{di}{\overline{Vsi}}} \qquad (3)$$

Where: di is the thickness and Vsi is the shear wave velocity of any layer of the Hefer Fm.

Figure 14 depicts examples of H/V spectral ratios for sites shown in Figure 13 together with the corresponding analytical transfer functions that were computed for the suggested 1D model to each site.

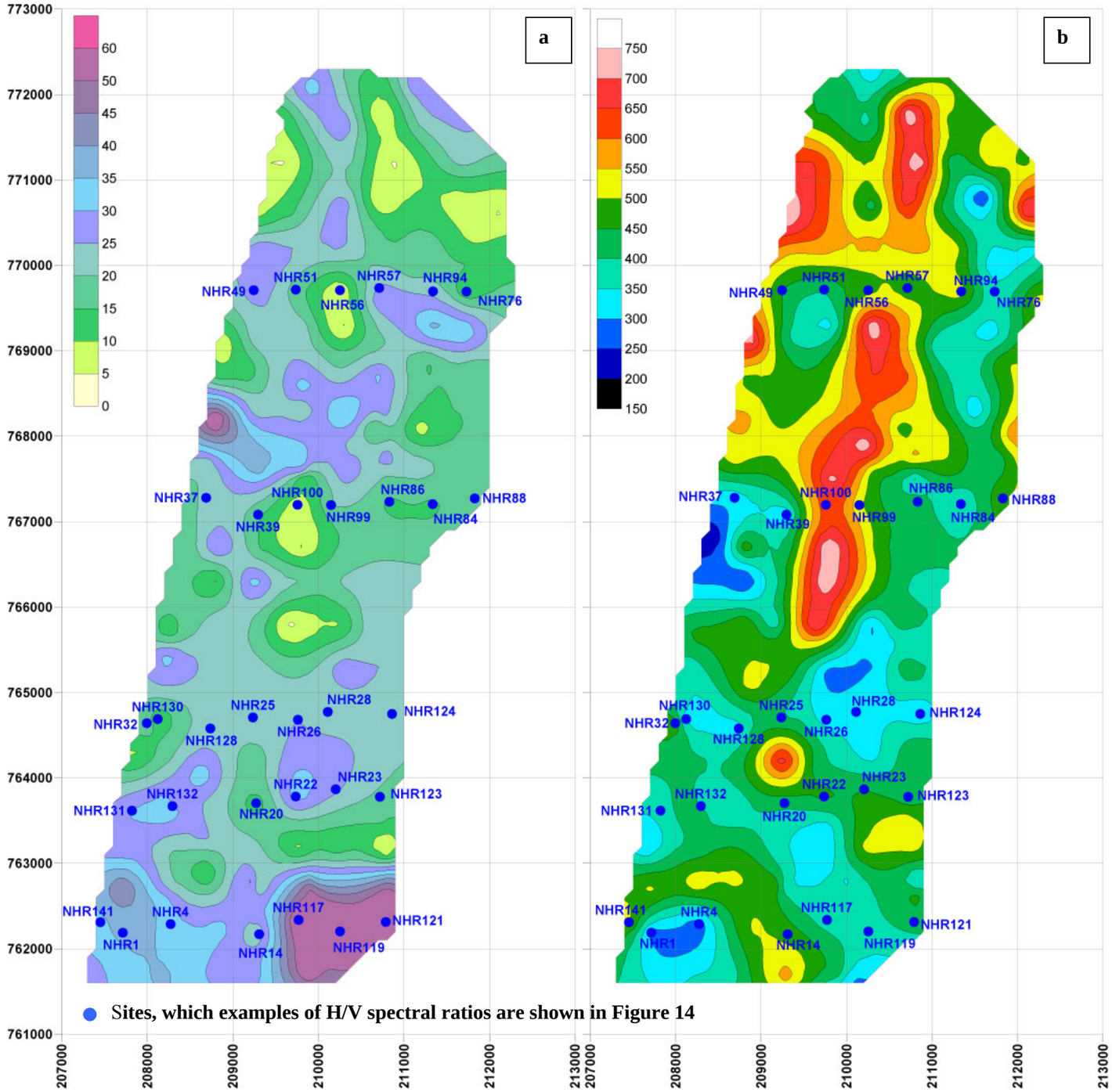

Figure 13. The thickness of sediments Hefer formations (a) and their average shear-wave velocity (b) obtained from microtremor measurement analysis.

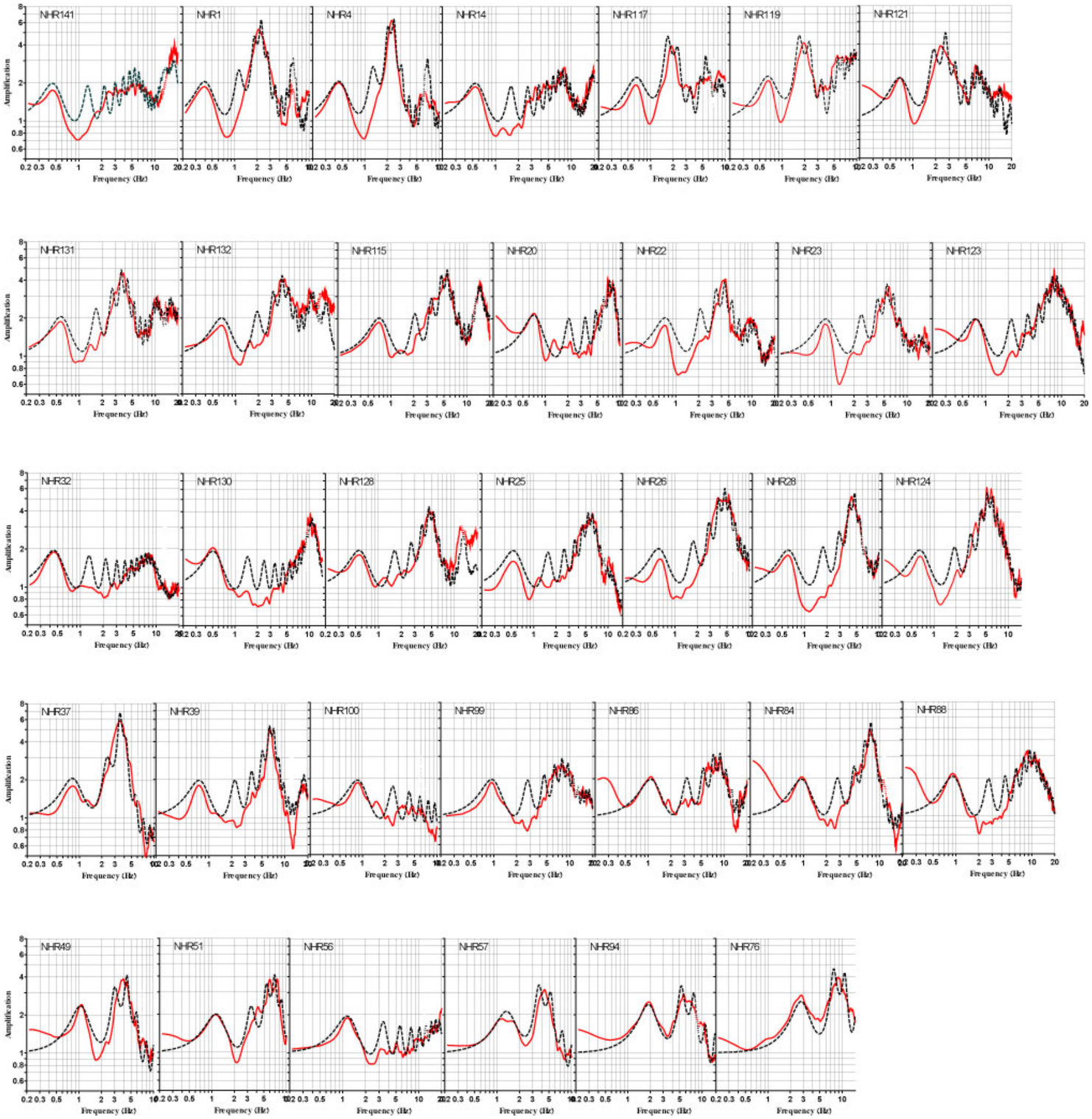

Figure 14. Comparison between the analytical transfer function (black dashed line) and experimental H/V spectral ratio (red line) obtained at sites are shown in Figure 13.

10. SEISMIC HAZARD MICROZONATION

We use H/V measurements together with available geological and geophysical information to construct a subsurface model for the investigated region. This model, in turn, may be used for estimating the expected site effects due to earthquakes. In the engineering practice, the aseismic building design and assessments of the earthquake risk refer to the site-specific acceleration (or displacement) spectrum. The design acceleration spectrum is essentially a representation of the maximum acceleration amplitudes for a prescribed probability of occurrence developed on a set of one degree of freedom oscillators with a given damping ratio. Since seismic activity in areas such as Israel is low, local acceleration data from strong earthquakes is insufficient to estimate directly the design acceleration spectrum.

A series of studies (Boore, 1983; Boore and Atkinson, 1987; Boore and Joyner, 1991 and others) described and demonstrated the stochastic method for synthesizing accelerograms of the S-wavetrain. Based on this Stochastic method, Shapira and van Eck (1993) developed the SEEH process (SEEH- Stochastic Estimation of the Earthquake Hazard) to predict the site specific acceleration response spectra computed for 10% probability of exceedence during an exposure time of 50 years and for a damping ratio of 5%.

The SEEH computations require information on several seismological parameters such as spatial distribution of seismogenic zones and their seismicity characteristics, stress drop, Q-values, seismic moment - local magnitude relationships, etc. Estimation of these parameters are based on seismological data (local and regional earthquake) provided by the local seismic networks. The SEEH applies Monte Carlo simulation to simulate the seismicity in the different seismogenic zones surrounding the investigated area over several thousands of years and applies the stochastic method to synthesize ground motions for each of the simulated events. At the final stage of the simulations, the synthetic horizontal accelerations propagate to the surface of the site through the soil layers constituting the site's sub-surface. The SEEH also incorporates the uncertainties associated with almost every parameter needed in the computations.

Based on the comparative analysis of the acceleration spectra computed, the study area is divided into 16 zones (Fig. 15). Soil-column models and acceleration spectra generalized for each zone are given in Table 3 and Fig. 16.

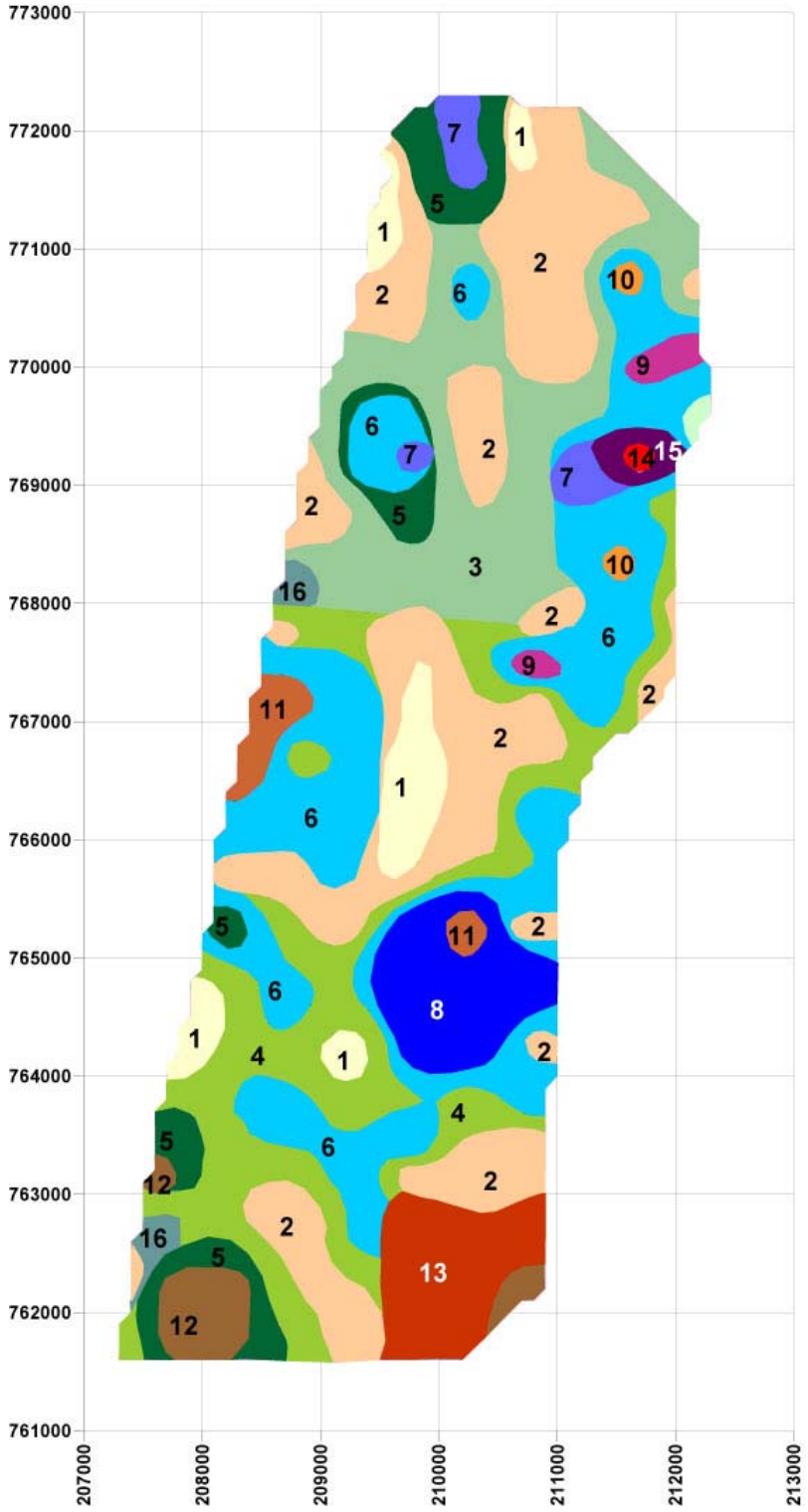

Figure 15. Seismic microzoning map of Nahariyya area.

For comparison, the designs spectra, required in the same area by the current Israel Standard 413 (IS-413), are plotted and for ground conditions that meet the BSSC (1997) soil

classification scheme. The shape of the hazard functions differ from those prescribed by the IS-413 code practically in all zones. The Israel code underestimates the acceleration in the different period ranges for the different zones.

Table 3 Soil column models for representative sites of zones.

Zone's number	Thickness m	Density gr/cm^3	Vs m/sec	Damping %
1	6	1.7	350	3
	5	1.9	720	3
	10	2.0	1200	0.2
	360	2.0	1020	0.2
	Half space	2.4	1900	
2	8	1.7	320	3
	18	1.6	690	3
	4	1.8	460	3
	10	2	1200	2
	115	2.0	750	2
	Half space	2.4	1900	
3	16	1.8	480	3
	7	1.9	700	3
	4	2	1200	2
	100	2	950	2
	Half space	2.4	1900	
4	4	1.5	160	3
	10	1.8	410	3
	9	1.8	550	3
	10	1.9	670	3
	20	2	1200	2
	360	2	1100	2
	Half space	2.4	1900	
5	7	1.7	370	3
	7	1.6	230	3
	18	1.9	625	3
	380	2	1100	2
	Half space	2.4	1900	
6	5	1.5	160	3
	7	1.7	380	3
	22	1.9	740	3
	7	2	1200	2
	115	2	900	2
	230	2	1100	2
	Half space	2.4	1900	

7	22	1.7	340	3
	20	2	1200	2
	180	2	1100	2
	Half space	2.4	1900	
8	9	1.5	183	3
	7	1.9	725	3
	9	1.8	500	3
	10	2	1200	2
	440	2	1100	3
	Half space	2.4	1900	
9	7	1.6	210	3
	5	1.9	650	3
	4	1.8	460	3
	100	2.0	960	2
	Half space	2.4	1900	
10	4	1.5	165	3
	2	1.6	270	3
	14	1.9	600	3
	42	2	1100	2
	Half space	2.4	1900	
11	5	1.7	350	3
	6	1.5	170	3
	10	1.8	580	3
	12	2	1200	2
	320	2	1100	2
	Half space	2.4	1900	
12	22	1.6	210	3
	10	1.9	620	2
	23	2	1200	2
	600	2	1100	1
	Half space	2.4	1900	
13	6	1.5	190	3
	5	1.9	670	3
	27	1.7	330	3
	20	1.9	610	3
	15	2	1200	1
	380	2	1100	12
	Half space	2.4	1900	
14	22	1.6	260	3
	10	1.9	650	3
	3	1.7	350	3
	50	2	1100	1
	Half space	2.4	1900	
15	19	1.7	330	3
	18	1.8	450	3
	80	2	1080	1
	Half space	2.4	1900	

16	12	1.9	640	3
	16	1.7	375	3
	30	1.9	740	3
	95	2	950	2
	Half space	2.4	1900	

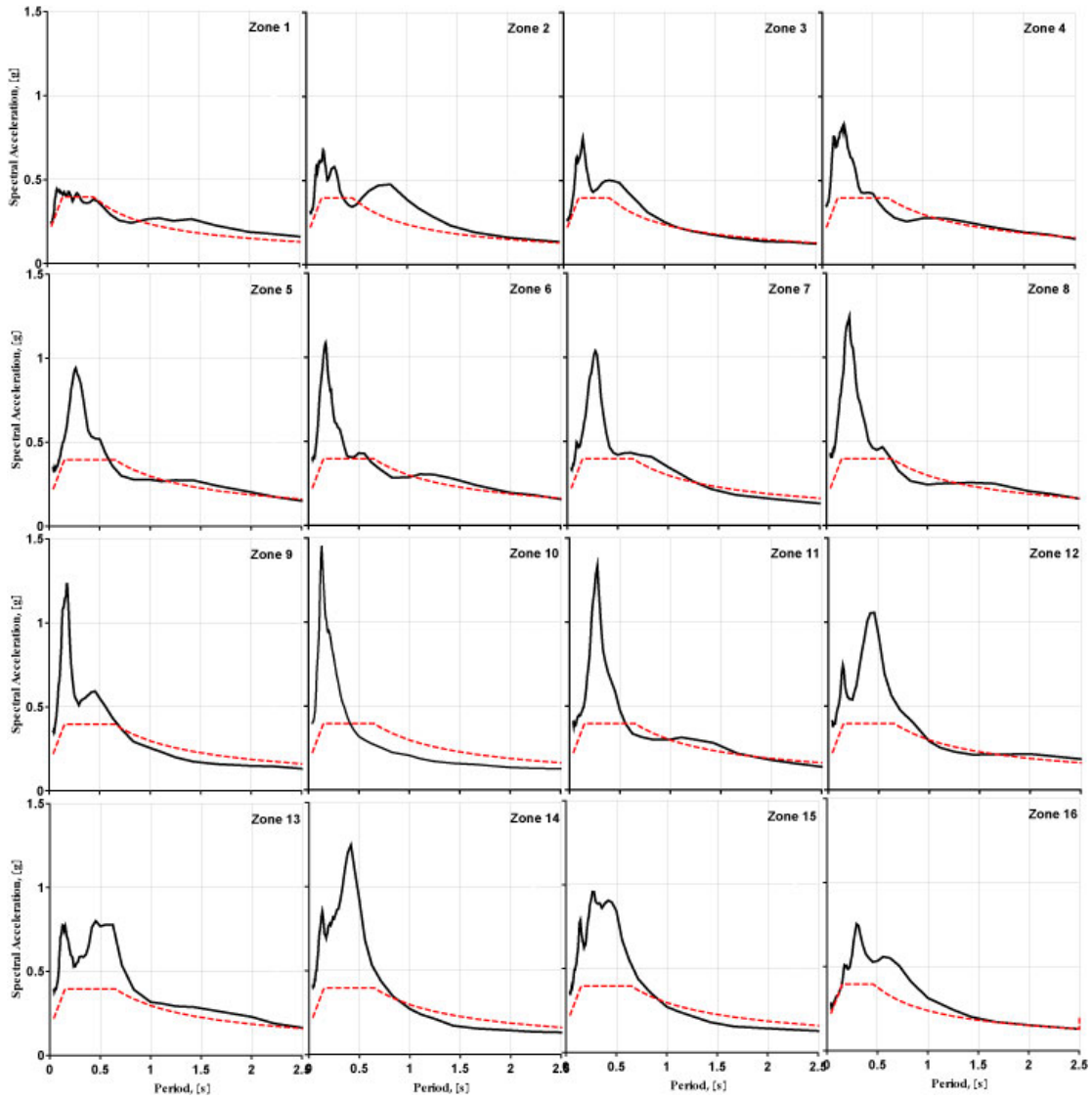

Figure 16 Spectral accelerations for each zone. Spectrum according to the Israel Building Code (PGA of 0.093) is indicated by the dashed line (included for reference).

CONCLUSIONS

Ground motion amplifications due to soft soils, common in urban areas, are a major contributor to increasing damage and number of casualties. The significant variability in the subsurface conditions across a study area and the relatively high costs associated with obtaining the appropriate information about the subsurface, may substantially limit proper hazard assessments. Direct information from strong motion recordings in urban areas is usually unavailable. The present report describes the seismic microzoning study in area from northern Akko to Nahariyya. In this study, we use noise recording conducted at 164 locations .

Our conclusions may be summarized as follows:

• The application of the Nakamura's method, using ambient noise measurements, seems to be very useful to study the regions with low natural seismicity. The fundamental frequencies and their associated H/V levels are in good correlation with the surface geology, and they are sensitive to the change of thickness in the soft deposits.

• The structure and properties of the underlying soils inferred only from geological and geophysical information may still lead to wrong assessments of site response, especially when based on 1D model. Reliable modeling to be used in site response analysis is obtained by combining different empirical approaches, supplemented with geophysical and geological data. Modelling allows estimating the thickness of the sediments at all measurement sites and constructing maps of the fundamental reflector depth, thickness and average shear-wave velocity of the sediments above shallow reflector.

• The ambient noise measurements enable identifying discontinuities in the subsurface and locate faults. In our study we reconstruct the faults previously traced by geological data and reveal some new. A higher density of H/V measurements would allow us to more accurately trace faults and identify new faults.

• Map of zones presented in the report in terms of the Uniform Hazard Site-specific Acceleration Spectra for a probability of exceedence of 10% during an exposure time of 50 years and a damping ratio of 5%, computed using SEEH procedure by applying the evaluated subsurface models may be useful for land use planning.

ACKNOWLEDGMENTS

Our thanks go to the Steering Committee for National Earthquake Preparedness for their financial support. A special thanks for Dr. Y. Zaslavsky for valuable suggestions and useful comments which helped to improve our work. We thank Y. Menahem for assistance in preparing this report.

REFERENCES

Ambraseys, N.N., 2009. Earthquakes in the Mediterranean and Middle East, A Multidisciplinary Study of Seismicity up to 1900. Cambridge University Press, Cambridge, UK, 800 pp.

Amiran, D.H.K., Arieh, E., Turcotte, T.; 1994: *Earthquakes in Israel and Adjacent Areas: Macroseismic Observations since 100 B.C.E*. Israel Exploration Journal, **2**, 261-305.

Avni, R., 1999. The 1927 Jericho earthquake, comprehensive macroseismic analysis based on contemporary sources, Ph.D. thesis, Ben Gurion University of the Negev, Beer-Sheva, Israel (in Hebrew with English abst.).

Avni, R.; Bowman, D.; Shapira, A.; Nur, A., 2002. Erroneous interpretation of historical documents related to the epicenter of the 1927 Jericho earthquake in the Holy Land. Journal of Seismology, 6, 469-476.

Bar Yosef, Y., 1967, The Hydrogeology of the Coastal Plain of Western Galilee, Tahal P.M. 557 (in Hebrew).

Ben-Menahem, A. (1979): Earthquake catalogue for the Middle East. 92 B.C. to 1980, Boll Geofis. Teor. Appl., 21, p. 260.

Borcherdt, R.D. and Gibss, J.F. 1976. Effects of local geological conditions in the San Francisco bay region on ground motions and the intensities of the 1906 earthquake, Bulletin of Seismological Society of America, 66 (No.2): 467-500.

Borcherdt, R., Glassmoyer, G., Andrews, M. and Cranswick, E.; 1989: Effect of site conditions on ground motion and damage, Earthquake spectra, Special supplement, Armenia earthquake reconnaissance report: 23-42.

Delgado, J., López Casado, C., Giner, J., Estévez, A., Cuenca, A., and Molina, S.; 2000: Microtremors as a exploration tool: application and limitations, Pure and Applied Geophysics, 157, 1445-1462.

Di Giulio, G., Cotnoi, C., Ohrnberger, M., Wathelet, M., and Rovelli, A, 2006. Deriving wavefield characteristics and shear-velocity profiles from to–dimensional small-aperture arrays analysis of ambient vibrations in a small0size alluvial basin, Colfiorito, Italy, Seism. Soc. Am., 96: 1915-1933.

Fleischer, L., and Gafsou, R., 2003: Top Judea Group – digital structural map of Israel. The Geophysical Institute of Israel, Report 753/312/03.

Garfunkel, Z., 1981. Internal structure of the Dead Sea leaky transform in relation to plate kinematics, Tectonophysics, 80, p. 81–108.

García-Jerez, A.; Luzón, F. ; Navarro, M.; Pérez-Ruiz, A. Characterization of the sedimentary cover of the Zafarraya basin, Southern Spain by means of ambient noise. Bull. Seism. Soc. Am. 2006, 96(3), 957-967

Gvirtzman, G., 1970, The Saqiye Group (Late Eocene to Early Pleistocene) in the Coastal Plain and Shefela Regions, Israel. IPRG Rep. 1022 and GSI Rep. OD/5/67.

Guidoboni, E., Comastri, A., Traina, G. 1994. Catalogue of ancient earthquakes in the Mediterranean area up to the 10th Century. ING-SGA, Bologna, Italy.

Guidoboni, E., Comastri, A. 2005. Catalogue of earthquakes and tsunamis in the Mediterranean area from the 11th to the 15th Century, INGV-SGA, ? Bologna, Italy.

Hamdache, M.; Palaez, J.A.; Yelles-Chauche, A.K. The Algiers, Algeria Earthquake (Mw 6.8) of 21 May 2003. Preliminary Report. Seism. Research Letters. 2004, 75(3), 360-367.

Hartzell, S. H.; Leeds, A.; Frankel, A.; Michael, J. Site response for urban Los Angeles using aftershocks of the Northridge earthquake. Bull. Seism. Soc. Am. 1996, 86,168-192.

Hinzen, K-G., Weber, B., and Scherbaum, F.; 2004: On the resolution of H/V measurements to determine sediment thickness, a case study across a normal fault in the lower Rhine embayment, Germany, J. Earthq. Engineer., 8 (6), 909-926.

Hofstetter, A., (Principal Investigator), 2008. Exploration of sedimentary layers and reconstruction of subsurface structure by ambient vibration measurements for microzoning of the Afek area. Scientific Report No. 508/388/08.

Hough, S. E.; Friberg, P.A.; Busby, R.; Field, E. F.; Jacob K.H.; Borcherdt R.D. Sediment-induced amplification and the collapse of the Nimitz Freeway. Nature. 1990, 344, 853-855.

Ibs-von Seht, M., and Wohlenberg, J.; 1999: Microtremor measurements used to map thickness of soft sediments. Bull. Seism. Soc. Am., 89, 250-259

Issar, A. and Kafri, U., 1972, Neogene and pleistocene geology of the Western Galilee Coastal Plain, Geological Survey of Israel, Bull., № 53, pp. 1-14, Jerusalem

Issar, A. and Picard, L., 1969, Sur le Tyrrhenian des cotes d'Israel et du Liban, Bull. Assoc. Fran. Etude Quarter. No. 18.

Iwata, T.; Hatayama, K.; Kawase H.; Irikura K., 1996. Site amplification of ground motions during aftershocks of the 1995 Hyogo-ken Nanbu Earthquake in several damaged zone – array observation of ground motions at Higashinada ward, Kobe city, Japan. Journal of Physics of the Earth,, 44(5), 553-61.

Jenkins, M. G. and Watts, D. G., 1969. Spectral analysis and its applications. Holden-Day, San Francisco, 1969, 471 pp.

Joyner, W.B. and Fumal, T.E. 1984. Use of measured shear-wave velocity for predicting geologic and site effects on strong ground motion, Proceedings of 8th World Conference on Earthquake Engineering, Vol.2: 777-783.

Katz O, 2004. Evaluation of earthquake induced landslide hazard in the city of Jerusalem area, Geology Survey of Israel Report GSI/12/2004, 34 pp (in Hebrew).

Kobayashi, K., Uetake, T., Mashimo, M., and Kobayashi, H.; 2000: Estimation of deep underground velocity structures by inversion of spectral ratio of horizontal to vertical component in p-wave part of earthquake ground motion. In: Proc. of 12th World Conference on Earthquake Engineering, Auckland, New Zealand, No. 2658.

Kuo, C-H., Cheng, D-S., Hsieh, H-H., Chang, T-M., Chiang, H-J., Lin, C-M and Wen, K-L., 2008. Comparison of thee different Methods in investigating shallow shear-wave velocity structures in Ilan, Taiwan, Soil Dyn. And Earth. Eng. 29 (2009), 133-143.

Liu, H. -P., Boore, D. M., Joyner, W. B., Oppenheimer, D. H., Warrick, R. E., Zhang, W., Hamilton, J.C., and Brown, L T., 2000. Comparison of phase velocities from array measurements of Rayleigh waves associated with microtremor and results calculated from borehole shear-wave velocity profiles, Seism. Soc. Am., 90: 666-678.

Maresca, R.; Galluzzo, D.; Del Pezzo, E. H/V spectral ratio and array techniques applied to ambient noise recorded in the Colfiorito basin, Central Italy. Bull. Seism. Soc. Am. 2006, 96(2), 490-505.

McGarr, A., Celebi, M., Sembera, E., Noce, T. and Mueller, C.; 1991: Ground motion at the San Francisco international airport from the Loma Prieta earthquake, sequence, Bull. Seism. Soc. Am., 81, 1923-1944.

Mero, D., 1983. Subsurface geology of Western Galilee and Zevulun. Plain. TAHAL, Tel-Aviv, Internal Report No. 04/83/48: 36 pp.

Nakamura, Y., 1989. A method for dynamic characteristics estimation of subsurface using microtremor on the ground surface. Quarterly Report of Railway Technical Research 30(1): 25-33.

Ozel, O., Cranswick, E., Meremonte, M., Erdik, M., and Safak, E., 2002, Site effects in Avcilar, west of Istanbul, Turkey, from strong-and weak-motion, Bull. Seism. Soc. Am., (Special Issue) 92(1): 499-508.

Parolai, S., Bormann, P. and Milkereit, C.; 2002: *New relationship between V_S, thickness of sediments, and resonance frequency calculated by the H/V ratio of seismic noise for the Cologne area (Germany)*, Bull. Seism. Soc. Am., *92 (*6), 2521-2527.

Pergalani, F., Pomeo, R., Luzi, L., Petrini, V., Pugliese, A., and Sano, T.; 2000 : *Criteria for seimic microzoning of a large area in central Italy*, In: Proc. of 12th World Conf. of Earth. Eng., Auckland.

Reinoso, E., and Ordaz, M.; 1999: *Spectral amplification for Mexico City from free-field recordings*, Earthquake Spectra, Vol. *15 N*o. 2, p. 273-295.

Shapira, A. and van Eck, T. Synthetic uniform hazard site specific response spectrum. Natural Hazard. 1993, 8, 201-205.

Shapira, A. and Avirav, V.; 1995: *PS-SDA Operation Manual*. Technical Report IPRG, The Institute for Petroleum Research and Geophysics, Z1/567/79, 24pp.

Salamon, A., Katz, O., Crouvi, O., 2009. Zones of required investigation for earthquake-related hazards in Jerusalem. Natural Hazards, DOI 10.1007/s11069-009-9436-6.

Sivan, D. (1996). Paleogeography of the Galilee Coastal Plain during the Quaternary. "Geological Survey of Israel Report 18/96". [In Hebrew, English summary]

Sivan, D., Gvirtzman, G., Sass, E., 1997, Quaternary Stratigraphy and paleogeography of the Galilee Coastal Plain, Israel, Quaternary Research 51, 280–294 (1999)

Tavron, B., Katz, O., Bar- Lavie, J., Segal, D., Leonard. G., 2007. Earthquake Loss Estimation for the City of Jerusalem: A Pilot Study of Implementing HAZUS Software. Report to the Committee for Earthquake Preparedness 41 pp. (in Hebrew).

Vered, M. and H. Striem (1976) The Safed earthquake of 1.1.1837 and its implications on risk evaluation in Israel, Isr. A.E.C, No. IA-LD-1-105.

Vered, M. and H. Striem (1977): A macroseismic study and the implications of structural damage of two recent major earthquakes in the Jordan Rift, Bull. Seism. Soc. Am., 67, 1607-1613.

Zaslavsky, Y., Gorstein, M., Aksinenko, T., Kalmanovich, M., Ataev, G., Giller, V., Dan, H., Giller, D., Perelman, N., Livshits, I and Shvartsburg, A.; 2006a: Interpretation of microtremor H/V ratio in multilayered media: a study at Haifa bay, Israel. In: Proc. of First European Conf. on Earthquake Engineer. and Seism., CD-Rom, Geneva, Sept., 2006a

Zaslavsky, Y., 2006b. Empirical determination of site local effect by ambient vibrations measurements for the earthquake hazard and risk assessment of Qrayot Haifa bay areas. Scientific Report No. 595/064/06.79 pp.

Zaslavsky, Y., 2007a. Use of ambient vibration measurements for reconstruction of subsurface structure along three profiles in the Zevulun Plain. Scientific Report No. 571/240/07.

Zaslavsky, Y., (Principal Investigator), 2007b. Sediment amplification from ambient noise excitation in the southern part of the Zevulun plain: a tool for reconstruction subsurface structure. Scientific Report No. 503/292/07.

Zaslavsky, Y.,, 2008. Empirical determination of site effects for seismic hazard assessment in Kishon Graben area near the Carmel Fault. Scientific Report No. 510/389/08.

Zaslavsky, Y., 2009. Site effects in the town of Akko: implications for seismic hazard assessment. Scientific Report No. 552/471/09.

יזרסקי, מ., 2006. סקר בשיטת הרפרקציה הסייסמית באזור מחלף "עכו דרום", 2006. דו"ח מג"י 260\203\06.